Int J Thermophys (2010) 31:966–974
DOI 10.1007/s10765-010-0732-x

Thermophysical Properties of Five Binary Copper–Nickel Alloys

Thomas Hüpf · Claus Cagran · Erhard Kaschnitz · Gernot Pottlacher

Received: 16 July 2009 / Accepted: 20 March 2010 / Published online: 13 April 2010

Abstract Thermophysical properties (e.g., specific enthalpy, heat of fusion, electrical resistivity, thermal volume expansion) are measured in the liquid phase up to very high temperatures by an extreme fast pulse-heating method. Heating rates of about $10^8\,\mathrm{K}\cdot\mathrm{s}^{-1}$ are applied by self-heating of wire-shaped metallic specimens with a current of approximately 10,000 A. Pure elements seem to be still close to thermal equilibrium as the obtained results are in good agreement with those obtained by static methods. However, this situation might be different for alloys. The rapid volume heating can shift diffusion-controlled phase transitions at heating to higher temperatures or even make them not noticeable anymore. The simple binary Cu–Ni system was chosen to test the heating rate dependence; this system is well known and shows complete miscibility in the liquid and solid ranges of interest. This study is a further step to test the performance of the fast pulse-heating method being applied to simple and more complex alloys. Measured results of enthalpy, heat of fusion, heat capacity, and electrical resistivity in the vicinity of the melting range are presented. The results of enthalpy and heat capacity agree with simple mixing rules. The measured electrical resistivity of different compositions is compared to results obtained by electromagnetic levitation measurements.

Keywords Binary alloy · Copper · Electrical resistivity · Heat capacity · Liquid metals · Nickel

T. Hüpf · C. Cagran · G. Pottlacher (✉)
Institut für Experimentalphysik, Technische Universität Graz, Petersgasse 16, 8010 Graz, Austria
e-mail: pottlacher@tugraz.at

T. Hüpf
e-mail: thomas.huepf@tugraz.at

E. Kaschnitz
Österreichisches Gießerei-Institut, Parkstraße 21, 8700 Leoben, Austria

1 Introduction

Microsecond pulse-heating experiments have been applied to a wide range of electrically conducting elements to obtain thermophysical properties at melting and in the liquid range. Despite the high heating rate (on the order of $10^8\,\mathrm{K}\cdot\mathrm{s}^{-1}$), the measured results agree well with data obtained by static and quasistatic methods. Recently, these methods have been extended to investigate alloys of technical interest. The more complex the alloys are the more non-equilibrium effects might influence the results of measurements with an increasing heating rate [1]. At the transition to the liquid phase and moderate heating rates, mass diffusion in the solid is more or less inhibited; the melting behavior can change dramatically. When the heating rate is further increased, the melting phase transition takes place almost without mass diffusion.

A simple binary alloy system (copper–nickel) with a small melting range and complete miscibility was chosen for this work to investigate different concentrations and to compare the results to properties of both pure elements, which have been extensively investigated by different authors [2–4]. The samples were die-cast and drawn to wires of 0.5 mm in diameter. Each composition (Cu85Ni15, $T_{\mathrm{sol}} = 1417\,\mathrm{K}$, $T_{\mathrm{liq}} = 1447\,\mathrm{K}$; Cu70Ni30, $T_{\mathrm{sol}} = 1472\,\mathrm{K}$, $T_{\mathrm{liq}} = 1520\,\mathrm{K}$; Cu55Ni45, $T_{\mathrm{sol}} = 1528\,\mathrm{K}$, $T_{\mathrm{liq}} = 1576\,\mathrm{K}$; Cu35Ni65, $T_{\mathrm{sol}} = 1599\,\mathrm{K}$, $T_{\mathrm{liq}} = 1638\,\mathrm{K}$; and Cu20Ni80, $T_{\mathrm{sol}} = 1656\,\mathrm{K}$, $T_{\mathrm{liq}} = 1678\,\mathrm{K}$; mass percent) was checked by chemical analysis (ICP spectral analysis, EDX). Solidus and liquidus temperatures close to equilibrium were partially measured by differential thermal analysis and are in very good agreement to literature values [5].

2 Experimental

During fast pulse-heating, wire-shaped specimens (diameter 0.5 mm, length 70 mm) are clamped in the center of a discharge circuit [6]. A capacitor (500 μF) is used as energy storage. The discharge vessel has windows for optical measurements (temperature, thermal expansion), and it provides the attachments for the voltage drop measurement along the wire performed by two knife-edge contacts which are directly touching the sample. The current is measured with an induction coil (Pearson-probe). The surface temperature is recorded with a high-speed pyrometer operated at 1570 nm (bandwidth approximately 85 nm). The melting plateau is used as a reference point, and temperatures are calculated with the assumption of a constant normal spectral emissivity throughout the liquid phase [7,8]. Thermal expansion is recorded by a fast CCD camera. The wire is backlit by a photoflash, and a magnified image is mapped on a multi-channel-plate, which acts as a fast shutter and amplifier [9].

As soon as the current starts, the sample is self-heating rapidly due to its ohmic resistivity. The high heating rate provides geometrical stability of the specimen for several tenths of microseconds even in the liquid phase; this timespan is long enough to perform the entire experiment. Additionally the short experimental time protects the specimen from chemical reactions.

The experimental parameters (e.g., charging voltage, neutral density filters for the pyrometer) were slightly different for each chemical composition of the alloy. An average of typically five individual measurements per composition was taken to calculate

the specific enthalpy, heat capacity, and electrical resistivity. Independently of that, 12 measurements for each composition were made to obtain thermal volume expansion from optical measurements.

3 Results

3.1 Enthalpy, Heat of Fusion, and Isobaric Heat Capacity

The specific enthalpy H as a function of time t was calculated using the equation,

$$H(t) = \frac{1}{m} \int_0^t I(\tau)\, U(\tau)\, \mathrm{d}\tau, \tag{1}$$

where m is the mass of the sample, I is the current, and U is the voltage drop.

The linear least-squares fits for the liquid phase are shown in Table 1 and Fig. 1. Figure 2 shows enthalpy values at 1750 K (dashed line in Fig. 1) as a function of nickel content. The heat of fusion ΔH was obtained as the difference of H between T_{sol} and

Table 1 Specific enthalpy, heat of fusion, and heat capacity of five Cu–Ni alloys

	$H\,(\mathrm{kJ\cdot kg^{-1}})$	Range	$\Delta H\,(\mathrm{kJ\cdot kg^{-1}})$	$c_p\,(\mathrm{J\cdot kg^{-1}\cdot K^{-1}})$
Cu85Ni15	$-26.1+0.545T$	$1447\,\mathrm{K} < T < 2000\,\mathrm{K}$	246.9	545
Cu70Ni30	$-182.9+0.663T$	$1520\,\mathrm{K} < T < 2000\,\mathrm{K}$	275.0	663
Cu55Ni45	$-137.5+0.658T$	$1576\,\mathrm{K} < T < 2000\,\mathrm{K}$	286.6	658
Cu35Ni65	$-175.6+0.685T$	$1638\,\mathrm{K} < T < 2000\,\mathrm{K}$	286.1	685
Cu20Ni80	$-148.7+0.701T$	$1678\,\mathrm{K} < T < 2000\,\mathrm{K}$	291.3	701

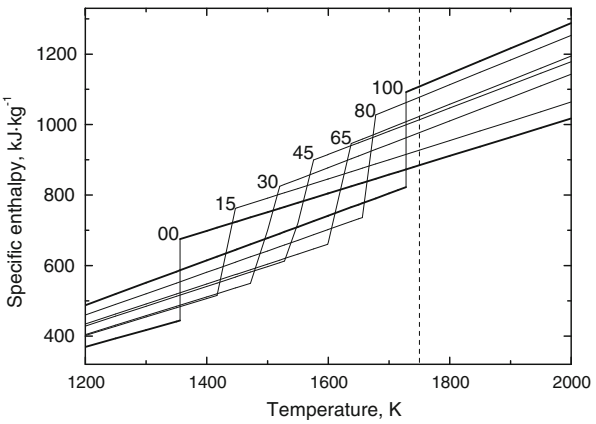

Fig. 1 Specific enthalpy of five Cu–Ni alloys, pure copper [2,3], and pure nickel [4] as a function of temperature; numbers refer to mass% nickel, *dashed line*: 1750 K (see Fig. 2)

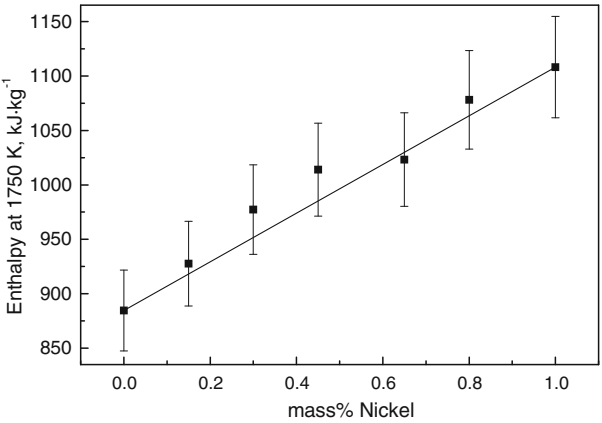

Fig. 2 Specific enthalpy of five Cu–Ni alloys, pure copper [2,3], and pure nickel [4] at 1750 K (as indicated by the *dashed line* in Fig. 1) as a function of nickel content; *solid line*: linear interpolation

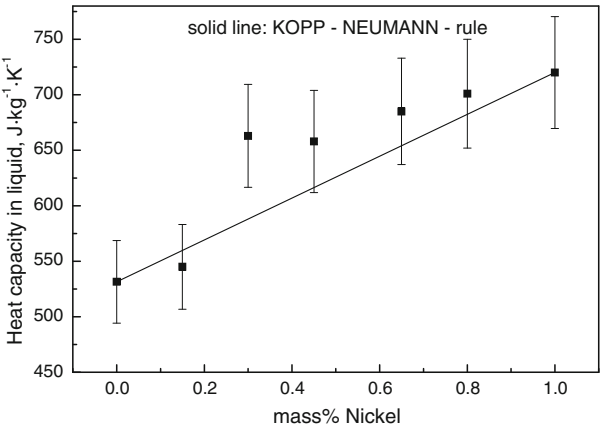

Fig. 3 Specific heat capacity of five Cu–Ni alloys, pure copper [2,3], and pure nickel [4] for the liquid phase as a function of nickel content; *solid line*: linear interpolation according to Kopp–Neumann rule

T_{liq} (subscript sol refers to solidus, liq to liquidus temperature). From its definition as the temperature derivative of enthalpy (under constant pressure), the isobaric heat capacity c_{p} can be obtained from the slope of the linear enthalpy fits (see Table 1). Figure 3 shows isobaric heat capacities for the liquid phase as a function of nickel content.

3.2 Resistivity

The electrical resistivity corresponding to the geometry at room temperature (initial geometry) ρ_{IG} was calculated using the equation,

$$\rho_{\mathrm{IG}}(t) = \frac{U(t)\pi r_0^2}{I(t)l}, \tag{2}$$

Table 2 Electrical resistivity ρ and $\Delta\rho$ of five Cu–Ni alloys; subindex IG: with initial geometry

	ρ_{IG} ($\mu\Omega \cdot$ m)	ρ ($\mu\Omega \cdot$ m)	Range	$\Delta\rho$ ($\mu\Omega \cdot$ m)
Cu85Ni15	$0.325 - 1.968 \times 10^{-4}T + 1.140 \times 10^{-7}T^2$	$0.358 - 2.599 \times 10^{-4}T + 1.515 \times 10^{-7}T^2$	$1200\,\mathrm{K} < T < 1417\,\mathrm{K}$	0.150
	$0.276 + 7.763 \times 10^{-5}T$	$0.233 + 1.459 \times 10^{-4}T$	$1447\,\mathrm{K} < T < 2000\,\mathrm{K}$	
Cu70Ni30	$0.587 - 2.292 \times 10^{-4}T + 1.097 \times 10^{-7}T^2$	$0.673 - 3.609 \times 10^{-4}T + 1.746 \times 10^{-7}T^2$	$1200\,\mathrm{K} < T < 1472\,\mathrm{K}$	0.161
	$0.560 + 3.211 \times 10^{-5}T$	$0.482 + 1.309 \times 10^{-4}T$	$1520\,\mathrm{K} < T < 2100\,\mathrm{K}$	
Cu55Ni45	$0.647 - 2.905 \times 10^{-4}T + 1.338 \times 10^{-7}T^2$	$0.808 - 5.290 \times 10^{-4}T + 2.370 \times 10^{-7}T^2$	$1200\,\mathrm{K} < T < 1528\,\mathrm{K}$	0.188
	$0.625 + 2.702 \times 10^{-5}T$	$0.584 + 9.953 \times 10^{-5}T$	$1576\,\mathrm{K} < T < 2100\,\mathrm{K}$	
Cu35Ni65	$0.545 - 7.253 \times 10^{-5}T + 6.149 \times 10^{-8}T^2$	$0.528 - 4.267 \times 10^{-5}T + 6.463 \times 10^{-8}T^2$	$1200\,\mathrm{K} < T < 1599\,\mathrm{K}$	0.221
	$0.688 + 4.538 \times 10^{-5}T$	$0.610 + 1.438 \times 10^{-4}T$	$1638\,\mathrm{K} < T < 2100\,\mathrm{K}$	
Cu20Ni80	$0.441 + 2.309 \times 10^{-5}T + 4.130 \times 10^{-8}T^2$	$0.425 + 5.167 \times 10^{-5}T + 4.549 \times 10^{-8}T^2$	$1200\,\mathrm{K} < T < 1656\,\mathrm{K}$	0.234
	$0.751 + 1.919 \times 10^{-5}T$	$0.635 + 1.397 \times 10^{-4}T$	$1678\,\mathrm{K} < T < 2100\,\mathrm{K}$	

where r_0 is the sample radius at room temperature and l is the length. Due to the thermal volume expansion, the sample radius changes during the heating process. This can be considered by the following equation:

$$\rho(T) = \rho_{IG}(T)\frac{D(T)^2}{D_0^2}, \tag{3}$$

where D_0^2 is the diameter at room temperature squared and D is the diameter at elevated temperature measured by the fast CCD-camera.

The least-squares fits for both ρ_{IG} and ρ are shown in Table 2. Fits are made with polynomials of the appropriate low order. Figure 4 shows the resistivity results corrected for thermal expansion including results obtained by electromagnetic levitation [10].

4 Discussion

4.1 Temperature and Melting Behavior

The traces of the pyrometer output signal exhibit a slightly sloped plateau at the melting transition. Figure 5 shows a single experiment for Cu55Ni45 where the slope is most significant. It should be noted that the temperature of the onset and end of this plateau is not directly correlated to the equilibrium solidus and liquidus temperatures. Slight changes in emissivity as well as the noise influence the signal. The middle of

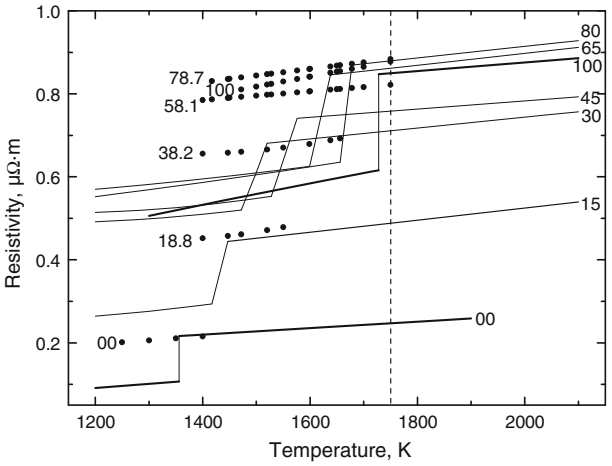

Fig. 4 Electrical resistivity of five Cu–Ni alloys, pure copper [2,3], and pure nickel [4] as a function of temperature; numbers refer to nickel content; *dots*: literature values measured by electromagnetic levitation [10], *open circles*: extrapolation of levitations measurements

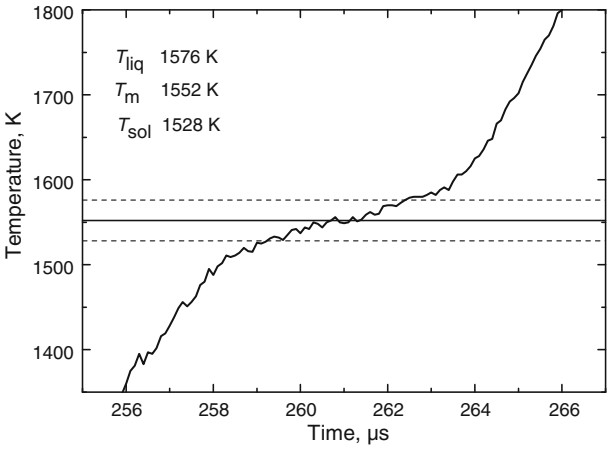

Fig. 5 Close up of the melting range in a temperature curve as a function of experimental time for a single experiment on Cu55Ni45. *Solid horizontal line*: arithmetic mean of solidus and liquidus temperature (*dashed lines*) which was assigned to the middle of the melting plateau

the plateau was used to assign the arithmetic mean of the solidus and liquidus temperatures of the phase diagram as a reference point for the temperature measurement. The temperature is calculated by Planck's law with the assumption of a constant normal spectral emissivity throughout the liquid phase [7]. Basak et al. [1] report for a binary NbTi-alloy that the heating rate (and grain size) can affect the melting behavior. Assuming a local equilibrium at the phase boundary at a moderate heating rate (max. $5 \times 10^3\ \mathrm{K \cdot s^{-1}}$), the melting range tends to be a plateau which converges to the liquidus temperature. For heating rates of approximately $10^8\ \mathrm{K \cdot s^{-1}}$ as used for this work, this approach is not applicable, as full diffusion in the liquid fraction at melting cannot

take place. For a full understanding of melting at these high speeds, measurements of normal spectral emissivity at melting and a theoretical approach to diffusionless melting have to be included in the future. Since the melting range of copper–nickel alloys is reasonably small, the influence of the uncertainty of the temperature reference point on the temperature measurement is limited.

4.2 Enthalpy and Heat Capacity

Figure 1 compares the traces of the five CuNi alloys with pure copper and pure nickel as a function of temperature. The dashed line (1750 K) represents the vertical section which is displayed in Fig. 2. Both figures show that the variation of enthalpy as a function of composition is more or less a linear function between the two pure elements.

The Kopp–Neumann rule predicts such a linear behavior for the specific heat capacity:

$$c_{p12} = \omega_1 c_{p1} + \omega_2 c_{p2}, \tag{4}$$

where ω_1 and ω_2 are the mass fractions of the constituent elements and c_{p1} and c_{p2} are their respective heat capacities. Figure 3 shows the specific heat capacity as a function of composition; within our uncertainties the results follow more or less the Kopp–Neumann rule. The specific heat capacity value at approximately 30 mass% Ni is higher than expected by the Kopp–Neumann rule. No explanation can be given for this behavior which indicates that the linear function in Fig. 2 is abandoned with increasing temperature.

4.3 Electrical Resistivity

Figure 4 shows the results of the electrical resistivity as a function of temperature for the range of chemical compositions in the copper–nickel binary alloy system. The resistivity of pure copper is significantly lower than an alloyed material. The resistivity increases rapidly with the amount of alloyed nickel and reaches a maximum at approximately 80 mass% nickel. The only results available in the literature with which to compare are obtained with different compositions by a levitation technique [10]. These values are partially gained in the undercooled liquid state. A comparison of the undercooled values to our results can be made by an extension to the regular liquid phase. There is a reasonable agreement between the quasi-static levitation measurement results and the results of this work, obtained by extreme fast heating.

A vertical section of the resistivity function at 1750 K is displayed in Fig. 6. It should be noted that the models for the electrical resistivity, which are discussed subsequently, refer to atoms and hence are described in mole fractions. The figure shows the obtained resistivity measurement results as well as a function obtained by an ideal solution model and the Nordheim rule converted into mass% to be consistent to prior text and images. A literature value for pure nickel [11] was added to the plot. The ideal

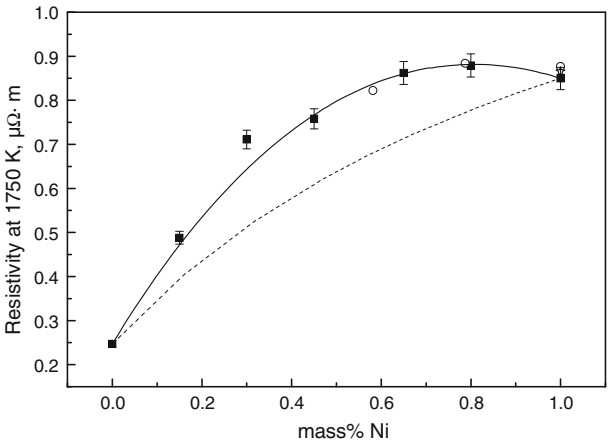

Fig. 6 Electrical resistivity of five Cu–Ni alloys, pure copper [2,3], and pure nickel [4] at 1750 K; *open circles*: literature values measured by electromagnetic levitation [10]; *open star*: literature value converted from [11]; *dashed line*: Eq. 5; *solid line*: Eq. 6

solution model calculates the resistivity by

$$\rho = \frac{\sum_i x_i Z_i \rho_i}{\sum_i x_i Z_i}, \tag{5}$$

where x_i is the concentration of element i, Z_i is the number of s-band electrons, and ρ_i is the resistivity of the pure component ($Z_{\mathrm{Cu}} = 1$ and $Z_{\mathrm{Ni}} = 2$). The Nordheim rule is calculated by

$$\rho = x_{\mathrm{Ni}}\rho_{\mathrm{Ni}} + (1 - x_{\mathrm{Ni}})\rho_{\mathrm{Cu}} + x_{\mathrm{Ni}}(1 - x_{\mathrm{Ni}})\rho_{\mathrm{Ni,Cu}}, \tag{6}$$

where $\rho_{\mathrm{Ni,Cu}}$ is a fit parameter which was found to be $95 \times 10^{-8}\,\Omega \cdot \mathrm{m}$.

Again, the resistivity value at approximately 32 at.% Ni is significantly higher than expected by the Nordheim rule and therefore was excluded from the fit.

5 Summary

Experimental results of enthalpy, heat capacity, and electrical resistivity of binary copper–nickel alloys are presented in this work. It shows that fast pulse-heating can be applied to binary alloys with a small melting range that are miscible in the solid and liquid. The results agree with that obtained by quasi-static measurements. However, for more complex alloys, the behavior of melting in very short time spans needs to be further analyzed.

6 Uncertainties

A detailed analysis of the estimation of uncertainties is given in [12]. Uncertainties calculated according to GUM [13] are as follows (relative uncertainties with a coverage factor $k = 2$): enthalpy in the solid state: $H_{\mathrm{sol}} \pm 6\,\%$; enthalpy in the liquid state: H_{liq}: 4 %; specific heat capacity: $c_{\mathrm{p,sol}}$: 7 %; $c_{\mathrm{p,liq}}$: 7 %; electrical resistivity with initial geometry: $\rho_{\mathrm{IG,sol}}$: 3 %; $\rho_{\mathrm{IG,\ liq}}$: 3 %; electrical resistivity: ρ_{sol}: 4 %; ρ_{liq}: 4 %.

A possible change of the normal spectral emissivity throughout the liquid phase is not considered [7].

Acknowledgments This work was supported by the Austrian Space Applications Programme (ASAP), the Basisprogramm of the Österreichische Forschungsförderungsgesellschaft mbH (FFG), and the Steirische Wirtschaftsförderungsgesellschaft mbH (SFG).

References

1. D. Basak, W.J. Boettinger, D. Josell, S.R. Coriell, J.L. McClure, S. Krishnan, A. Cezairliyan, Acta Mater. **47**, 3147 (1999)
2. C. Cagran, A. Seifter, G. Pottlacher, *Thermophysical Properties of Solid and Liquid Copper,* Schriften Des Forschungszentrums, Jülich Ser. Energy Technol. **15**, 763 (2000)
3. G.Nussbaumer, *Weiterentwicklung der zeitaufgelösten Expansions-und Spannungsmessung bei Mikrosekunden-Pulsheizexperimenten–Bestimmung thermophysikalischer Daten von Kupfer und Gold*. Diploma-Thesis, Institute of Experimental Physics, Graz University of Technology (1993)
4. B. Wilthan, C. Cagran, G. Pottlacher, Int. J. Thermophys. **25**, 1519 (2004)
5. S.A. Mey, Calphad **16**, 255 (1992)
6. E. Kaschnitz, G. Pottlacher, H. Jäger, Int. J. Thermophys. **13**, 699 (1992)
7. T. Hüpf, C. Cagran, G. Pottlacher, *Pyrometrische Temperaturmessung – Einfluss des Emissionskoeffizienten auf die Bestimmung thermophysikalischer Daten*. Proceedings: TEMPERATUR2009 (2009)
8. G. Pottlacher, A. Seifter, Int. J. Thermophys. **23**, 1281 (2002)
9. B. Wilthan, H. Reschab, R. Tanzer, W. Schützenhöfer, G. Pottlacher, Int. J. Thermophys. **29**, 434 (2008)
10. G. Lohöfer, J. Brillo, I. Egry, Int. J. Thermophys. **25**, 1535 (2004)
11. E. Kaschnitz, J.L. McClure, A. Cezairliyan, Int. J. Thermophys. **15**, 757 (1994)
12. C. Cagran, T. Hüpf, B. Wilthan, G. Pottlacher, High Temp. High Press. **37**, 205 (2008)
13. *Guide to the expression of uncertainty in measurement* (ISO, Geneva, 1993)